ELSEVIER

Chemical Physics 280 (2002) 309–329

Chemical Physics

www.elsevier.com/locate/chemphys

Dissociation of multiply ionized alkanes from methane to *n*-butane due to electron impact

Pengqian Wang*, C.R. Vidal

Max-Planck-Institut für extraterrestrische Physik, Postfach 1312, 85741 Garching, Germany

Received 23 January 2002

Abstract

The dissociation of up to triply ionized alkanes from methane to *n*-butane has been studied through electron impact ionization at an electron energy of 200 eV. The ionic fragments are recorded by a covariance mapping technique using a focusing time-of-flight mass spectrometer. The absolute cross-sections for the numerous dissociation channels of all the alkane monocations and dications, as well as propane and *n*-butane trications have been obtained. All the alkane dications are unstable and dissociate mostly into ion pairs, in which the production of proton pairs is found to be a major dissociation channel. The ionic products from the dissociation of ethane, propane and *n*-butane dications have a similar distribution, in which the first few abundant ion species are H^+, CH_3^+, $C_2H_3^+$ and $C_2H_2^+$. The total single ionization cross-sections agree well with the results of the binary-encounter-Bethe method. The distortion of the ion coincidence islands has been explained as due to the deviation from the space focusing condition of the mass spectrometer. Metastable decays, such as $C_3H_5^{2+} \rightarrow CH_3^+ + C_2H_2^+$ in propane and $C_4H_{10}^+ \rightarrow C_3H_7^+ + CH_3$ in *n*-butane have been observed and identified using the initial and final angles of the decay traces. © 2002 Elsevier Science B.V. All rights reserved.

1. Introduction

The dissociation of multiply ionized molecular ions is very interesting in the research areas such as plasma physics and planetary atmospheric chemistry, and has been extensively investigated in recent years (for example, [1–14]). The study of the dissociation dynamics of multiply ionized molecular ions provides valuable information on the electronic states and potential energy surfaces of the parent ions, and increases our knowledge on the various bonds between the atoms. Different experimental methods, such as fast ion beam collision [4–6], neutral beam collision [7], photoionization [8], intense laser field [9–11] and electron impact [12–14] have been used to excite and ionize molecules or molecular ions of lower stages. Among these methods electron impact has been widely used, since electron impact ionization of molecules is considered as one of the fundamental processes in molecular physics [15,16]. Also the cross-section data of electron impact ionization are currently urgently needed in the areas such as

* Corresponding author. Tel: +49-89-30000-3827; fax: +49-89-30000-3569.

E-mail address: pqw@mpe.mpg.de (P. Wang).

0301-0104/02/$ - see front matter © 2002 Elsevier Science B.V. All rights reserved.
PII: S0301-0104(02)00508-6

plasma modeling in semiconductor manufacturing [17,18]. Under electron impact the molecules are mainly ionized into lower stages, i.e. into monocations or dications, which allows us to study the dissociation dynamics of relatively low states of the molecules.

Small alkane molecules are prototypes for polyatomic organic molecules and are important in many research fields in chemical physics. They are also interesting in astrophysics since they are important constituents in the planetary and cometary atmospheres. The dissociation of singly and multiply ionized alkanes has been studied for more than 40 years. Earlier works are mainly on the dissociation of alkane monocations [19–24], among which propane is extensively studied and it is considered as a good example for the quasi-equilibrium theory of mass spectra [19]. Methane monocations have also been studied through neutral beam collision by Kupriyanov and Perov [25] and through proton impact by Ben-Itzhak et al. [6]. The study on the dissociation of multiply ionized molecules requires one to distinguish the different dissociation pathways with coincidence techniques, such as photoion–photoion coincidence [26], photoelectron–photoion–photoion coincidence [27] and covariance mapping [28]. Methane dications have been studied through proton impact by Ben-Itzhak et al. [6], through electron impact by Backx and Van der Wiel [29] and McCulloh et al. [30], and through photoionization by Fournier et al. [26]. The results of these experiments generally agree with each other except those using very low excitation energies. Although some works have been done on the dissociation of alkane dications, the absolute cross-sections for the different dissociation channels are still unavailable, and the relative cross-sections have only been measured in methane [6,26,29,30]. The absolute cross-sections for a wide range of dissociation channels of the alkane ions are needed. They are important in understanding the excitation distribution and the consecutive dissociation of these molecular ions.

In this paper, we report the dissociation of small alkanes from methane to *n*-butane after single, double and triple ionization using electron impact at an energy of 200 eV. This energy is used because we expect that like in other molecules, such as CO_2 [13], CO [14], N_2 and O_2 [31], at this energy most dissociation channels may have cross-sections close to their maximums, so that they can be easily detected. Also above 200 eV the relative cross-sections of most of the dissociation channels may have no significant variations any more [13,14,31]. The experimental setup and the methods used to deduce the cross-sections for the different dissociation channels are described in Section 2. The covariance mapping technique is used, accompanied by a focusing time-of-flight mass spectrometer. In Section 3, the various cross-sections are presented, including the partial cross-sections for electron impact ionization, and the cross-sections for the different dissociation channels of the alkane cations. The ionic product distribution from the dissociation of alkane dications is also shown. The distortion of the ion coincidence islands observed in our experiment has been investigated. Some signatures of metastable decays are observed and identified using the initial and final angles of the decay traces.

2. Experimental method

The experimental apparatus has been described elsewhere [32,33], thus only a brief description is given here. A crossed beam geometry is used. The molecular beam is provided by a continuous gas flow from a long needle with 0.4 mm diameter passing through a skimmer with an orifice of 0.75 mm diameter. The electron beam is provided by a pulsed (100 ns) electron gun. The tip of the needle is 20 mm above the skimmer and the skimmer is 60 mm above the electron beam. The two beams cross each other at right angles, and the interaction region is believed to be less than $4 \times 4 \times 4$ mm^3. At about 100 ns after the electron beam the ions are extracted into a specially designed focusing time-of-flight (FTOF) mass spectrometer [32], which is modified from a normal Wiley–McLaren mass spectrometer [34]. The shield plates in the interaction region of the FTOF mass spectrometer make the extraction mesh act as a plane-convex lens, which focuses the ions close to the axis of the mass spectrometer and reduces the divergence of

the ion beam. The flight tube of the FTOF mass spectrometer consists of two tubes of equal length with a fine mesh in between. If the voltage applied on the mesh is 1.25–1.40 times as high as that on the flight tubes, the mesh will serve as a spherically symmetric lens and focus the ions onto the center of the microchannel plate detector (Galileo 3040). In the present experiment, the voltage on the flight tubes is set to be −2.54 kV, and on the focusing mesh −3.20 kV. The pulsed voltage on the extraction mesh is −1.20 kV. These voltages are approximately twice as high as those we used previously [32,33], so that we can collect all the energetic ions. The bias voltage on the microchannel plate is −3.60 kV, and the ion energy at the front surface of the microchannel plate is 3.2 keV/charge. Simulation of the ion trajectory [32] has shown that using the present voltage setting the ions with initial energies as high as 25 eV/charge can be collected with the same efficiency as the thermal ions. The kinetic energies of the energetic ions produced by electron impact ionization of the alkanes from methane to *n*-butane have been measured by a number of authors [35–39]. All the peak values in the kinetic energy distributions are generally less than 5 eV, they are well within the collecting ability of the present experiment. The non-discriminative collection of the ions can be experimentally verified by varying the voltages on two deflectors in the flight tube. The deflectors are located in the first tube and have a length of about 20% of the two flight tubes. The output of the microchannel plate is preamplified and then sent to a constant fraction discriminator. The threshold of the discriminator is set properly so that the noise is eliminated and all the ion signals are passed. The ion signals are recorded by a fast multichannel scaler with a time resolution of 0.5 ns. The alkanes are purchased from Linde AG with a stated purity of 99.95%. The experiment is performed at a repetition rate of 4 kHz with a total number of 10^8 pulses for each gas.

In order to study the different dissociation channels of multiply ionized molecules, the ionic fragments must be recorded in coincidence. The two-dimensional covariance mapping technique developed by Frasinski et al. [28] has been used in our experiment. The principle of this technique is described briefly as follows. Let $X_n(i)$ be the single pulse TOF spectrum of the nth pulse, where i is the time bin of the multichannel scaler. The covariance function of the single pulse spectrum is described by

$$C(i,j) = \sum_{n=1}^{N} X_n(i)X_n(j) - \frac{1}{N}\sum_{n=1}^{N} X_n(i)\sum_{n=1}^{N} X_n(j). \tag{1}$$

Here N is the total number of pulses. The first term of Eq. (1) is the total coincidence between the ions, and the second term corresponds to the false coincidence, in which the coincident ions are produced from different dissociation events. As shown in Eq. (1), the false coincidence is proportional to the autocorrelation function of the single count spectrum, i.e. the accumulated single pulse spectrum $\sum_{n=1}^{N} X_n(i)$. Removing the false coincidence is often achieved in an alternative way like that used by Bruce et al. [40] and Ben-Itzhak et al. [6,41]. Briefly, the autocorrelation function of the single count spectrum is normalized so that its count in a completely false coincidence area (such as $C_3H_7^+ + C_4H_{10}^+$ in *n*-butane) is equal to that in the same area of the total coincidence, and then it is subtracted from the total coincidence. Statistically as shown in Eq. (1) the normalization factor should be close to the reciprocal of the total number of pulses. In our experiment, this factor is between 9.95×10^{-9} and 1.00×10^{-8}, which is in good agreement with this prediction. If the covariance function of the single pulse spectrum is plotted in a two-dimensional coordinate system, where the x-axis displays the faster ions and the y-axis displays the slower, we will get a covariance map, which is a powerful method to distinguish the different dissociation channels of multiply ionized molecules.

In the present study the partial ionization cross-sections of methane and ethane are obtained by simply normalizing the total ion counts to the total cross-sections measured previously in our laboratory. They are 3.34×10^{-16} cm^2 for methane [33] and 5.47×10^{-16} cm^2 for ethane [36]. This is because the total electron impact ionization cross-sections of small molecules have been well established. They can be measured by

simple and reliable apparatuses such as parallel plate ion collectors [42,43]. The partial cross-sections for propane and *n*-butane are obtained by normalizing the ion counts to a well-known gas such as argon. At first, argon is used and the count of Ar^+ is recorded. Then propane or *n*-butane is used with the same backing pressure as argon, and all other experimental conditions are kept unchanged. The pressure of the gas in the chamber above the needle is kept low enough so that the gas flow is in the effusive flow regime. The absolute cross-section of a particular ion, e.g. C^+, is given by

$$\sigma(C^+) = \frac{I(C^+)}{I(Ar^+)}\sigma(Ar^+), \tag{2}$$

where I is the ion count in the single count spectrum. Argon is used as the reference gas because its cross-sections have been well established. The result of Straub et al. [44], which is $\sigma(Ar^+) = 2.18 \times 10^{-16}$ cm^2, is used in the present work.

The absolute cross-section for the production of a particular ion pair, e.g., $C^+ + H^+$, can be obtained by

$$\sigma(C^+ + H^+) = \frac{n_{\text{coincidence}}(C^+ + H^+)}{n_{\text{total}} T \eta}\sigma_{\text{total}}. \tag{3}$$

Here $n_{\text{coincidence}}$ is the ion-pair count inside the corresponding island on the covariance map, n_{total} is the total number of ion counts in the single count spectrum, and σ_{total} is the total cross-section of the molecule. T is the total transmission of the meshes in the mass spectrometer, and η is the detection efficiency of the microchannel plate. The value of T is taken from the open area ratio in the manufacture's manual, which is 58.1% and agrees with the optical transparency of the meshes. For η we use the open area ratio from the manufacture's manual, which is 54.5%. It has been shown that the detection efficiency of the microchannel plate is equal to its physical open area ratio [44–46].

The highest-order ionization in our experiment is found to be the triple ionization, therefore all the detected ions are produced from alkane monocations, dications or trications. The possible dissociation channels for these ions are listed in Table 1, which have been divided into five groups according to the charges of the parent ion and the ionic fragments. Since no trication has been directly observed in our experiment, the channels that produce $C_mH_n^{3+}$ are omitted. The neutral fragments are not recorded in the present experiment. For the sake of brevity, we use the symbol "N" to stand for all the neutral fragments if they exist, and "N" vanishes if there is no neutral product. The stabilization channels, in which no dissociation of the alkane cations occurs, are also included in the first and second channel. The cross-section for each dissociation channel is denoted in the last column. The subscript of σ is the charge of the parent ion, and m, n, etc., are sequentially the number of C and H atoms in the ionic products. It is remarkable that the fifth channel in Table 1, i.e. the equal charge separation channel, may be important for the dissociation of trications. To measure this channel a three-dimensional coincidence technique is required, which is at present not available in our work. However, since this channel occurs at a higher stage of ionization, its cross-section $\sigma_3(m,n,i,j,k,l)$ is expected to be at least one order of magnitude smaller than $\sigma_2(m,n,i,j)$ [13]. As a result, we neglect its contribution to the islands $C_mH_n^+ + C_iH_j^+$, etc., and assume that Eq. (3) gives $\sigma_2(m,n,i,j)$. Also $\sigma_3(m,n,i,j)$ can be directly obtained from the count of the corresponding island on the covariance map. The remaining cross sections, i.e. $\sigma_1(m,n)$ and $\sigma_2(m,n)$, are for the channels that produce only one ionic fragment. They can be derived as follows. Since any ionic species detected in the experiment should come from one or more channels listed in Table 1, let $\sigma^+(m,n)$ and $\sigma^{2+}(m,n)$ be the cross-sections of $C_mH_n^+$ and $C_mH_n^{2+}$, which are given by Eq. (2), we have the sum rules

Table 1
Possible dissociation channels for alkane monocations, dications and trications

Parent ion	Dissociation channel	Cross-section
$C_xH_{2x+2}^+ \rightarrow$	$C_mH_n^+ + N$	$\sigma_1(m,n)$
$C_xH_{2x+2}^{2+} \rightarrow$	$C_mH_n^{2+} + N$	$\sigma_2(m,n)$
	$C_mH_n^+ + C_iH_j^+ + N$	$\sigma_2(m,n,i,j)$
$C_xH_{2x+2}^{3+} \rightarrow$	$C_mH_n^{2+} + C_iH_j^+ + N$	$\sigma_3(m,n,i,j)$
	$C_mH_n^+ + C_iH_j^+ + C_kH_l^+ + N$	$\sigma_3(m,n,i,j,k,l)$

"N" denotes the neutral fragments if they exist.

$$\sigma^{+}(m,n) = \sigma_1(m,n) + \sum_{i,j}(1+\delta_{mi}\delta_{nj})\sigma_2 \times (m,n,i,j) + \sum_{i,j}\sigma_3(i,j,m,n) + \sum_{i,j,k,l}(1+\delta_{mi}\delta_{nj}+\delta_{mk}\delta_{nl})\sigma_3 \times (m,n,i,j,k,l), \quad (4)$$

$$\sigma^{2+}(m,n) = \sigma_2(m,n) + \sum_{i,j}\sigma_3(m,n,i,j). \quad (5)$$

Here δ_{mi}, etc., are the Dirac symbols, i.e. $\delta_{mi} = 1$ if $m = i$, otherwise $\delta_{mi} = 0$. The cross-section $\sigma_3(m,n,i,j,k,l)$ may be smaller than $\sigma_1(m,n)$ by several orders of magnitude since its ionization is two stages higher. Therefore we neglect the last term in Eq. (4). After doing this $\sigma_1(m,n)$ and $\sigma_2(m,n)$ are ready to be calculated from Eqs. (4) and (5).

The ion counts from the background gases are measured without the alkane molecule. They are usually less than 5% of the total counts of the alkane and are subtracted from the covariance map. The error in the cross-sections of single ions relative to the total cross-section is expected to be 8%, which originates mainly from the data fluctuations, the gas pressure stability and the counts from the isotopes. The normalization of the cross-sections causes an error of about 4%. As a result, the error in the cross-sections of single ions is believed to be generally 10%. For minor ions it may be about 15%. The error in the cross-sections for ion pairs is mainly due to the subtraction of the false coincidence, the transmission of the meshes and the detection efficiency of the microchannel plate. In our experiment, the counting rate is set to be about only 1 ion per pulse, the false coincidence cannot cause a large error. This can be confirmed by studying the shape of the islands on the covariance map. The error in the total cross-section (10%) is also an error source for the cross-sections for ion pairs. As a result, we expect that the total error in the cross-sections for ion pairs is generally about 20%. A minor part of the islands on the diagonal of the covariance map, i.e. $C_xH_{2x+2}^{2+} \rightarrow 2C_mH_n^{+} + N$, is suppressed by the dead time (about 6 ns) of the discriminator and the multichannel scaler. We made a compensation for these islands by assuming that the peaks of the islands are flat near the diagonal. This is normally true because in a time-difference spectrum, e.g. a photoion–photoion coincidence spectrum the ion-pair count generally has a flat top [26]. We expect that the error in the cross-sections for the islands on the diagonal is about 25%. For the dissociation channels that produce only one ionic fragment, since the cross-sections are derived indirectly, the error is expected to be about 25%, and it may be more for very weak channels.

3. Results and discussions

3.1. Cross-sections for electron impact ionization and dissociative ionization

The TOF mass spectra of methane, ethane, propane and *n*-butane at the electron energy of 200 eV are shown in Fig. 1. Note that $C_3H_n^{2+}$ ($n = 2$–5) in propane and $C_4H_n^{+}$ ($n = 0$–10) in *n*-butane have been amplified and shifted to show the details. All the mass peaks are well resolved except some minor ions in *n*-butane. Some small mass peaks, such as $m = 17$ in methane, $m = 16$, 31 in ethane, $m = 16$, 30, 45 in propane and $m = 16$, 30, 44, 59 in *n*-butane are due to the isotopic impurities of ^{13}C. The widths of CH_n^{+} ($n = 0$–3) in ethane, propane and *n*-butane are significantly broader than those in methane due to their larger initial kinetic energies. Similar broadening of $C_2H_n^{+}$ ($n = 0$–5) in propane as well as $C_2H_n^{+}$ ($n = 0$–5) and $C_3H_n^{+}$ ($n = 0$–7) in *n*-butane can also be seen.

As mentioned above, the non-discriminative collection of the ions with respect to their initial kinetic energies can be tested by the two deflectors in the mass spectrometer. The deflection curves for methane [33] and ethane [36] have been shown in previous publications. In the present experiment only the collection efficiencies of propane and *n*-butane are tested, which has been done by setting the voltage on one deflector equal to that on the flight tubes (−2.54 kV) and changing the voltage on the other deflector. For both propane and *n*-butane all the deflection curves show good flat tops. The ion counts for $\sum C_3H_n^{+}$ ($n = 0$–8),

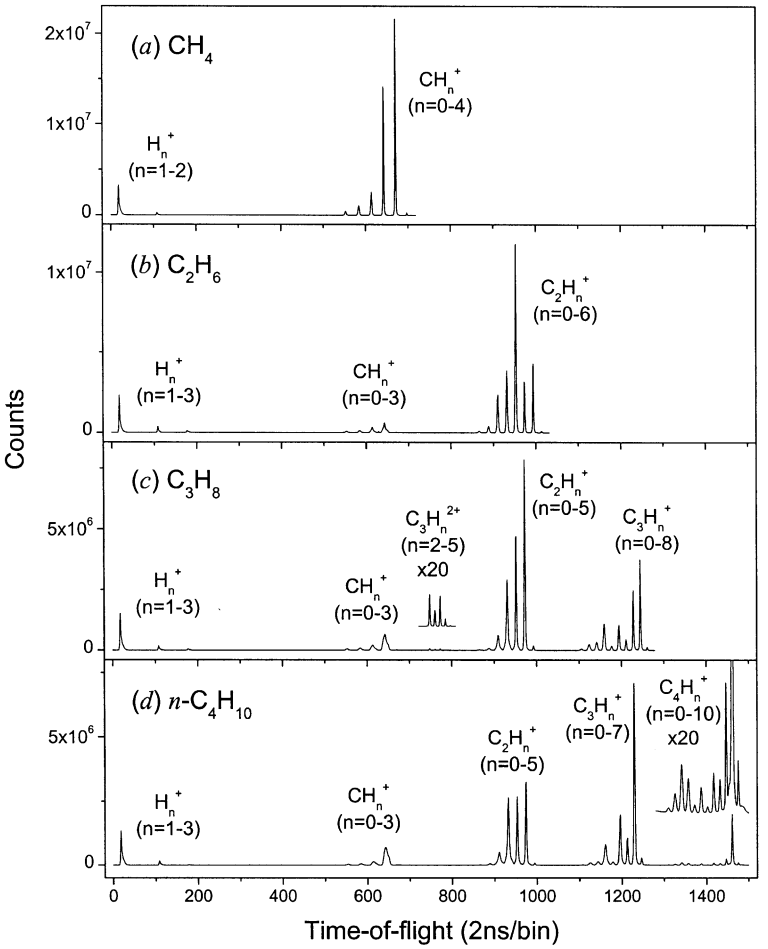

Fig. 1. The time-of-flight mass spectra of: (a) methane; (b) ethane; (c) propane; (d) *n*-butane. The electron energy is 200 eV.

$\sum C_2H_n^+$ ($n = 0$–5), $\sum C_3H_n^{2+}$($n = 2$–5), $\sum CH_n^+$ ($n = 0$–3), H_3^+, H_2^+ and H^+ in propane, as well as the ion counts for $\sum C_4H_n^+$ ($n = 0$–10), $\sum C_3H_n^+$ ($n = 0$–7), $\sum C_2H_n^+$ ($n = 0$–5), $\sum CH_n^+$ ($n = 0$–3), H_3^+, H_2^+ and H^+ in *n*-butane stay nearly constant while the voltage on either of the deflectors varies between −1.7 and −3.5 kV. This implies that the ion beam diameter is sufficiently smaller than that of the effective area of the detector. Therefore we conclude that all the ions produced in the ionization region have been detected with the same efficiency.

The cross-sections for electron impact ionization and dissociative ionization of methane are listed in column *a* of Table 2. The discrepancy between the present result and our previous cross-sections [33] is within 9%, which is mainly caused by the reproducibility of the experiment and the small modifications of the apparatus. Comparisons between our data and those from Straub et al. [47], Tarnovsky et al. [48], Orient et al. [49] and Chatham et al. [50] have been done elsewhere [33], which shows that all the previous data except those of Straub et al. have smaller cross-sections for small ions. Our result agrees well with those of Straub et al. because both experiments have made efforts to detect the energetic ions.

The cross-sections for electron impact ionization and dissociative ionization of ethane are listed in column *a* of Table 3. Although dications such as

Table 2
The cross-sections (10^{-19} cm^2) for electron impact ionization and dissociative ionization of methane (*a*), for the dissociation channels $CH_4^+ \rightarrow C_mH_n^+ + N$ (*b*), and for the dissociation channels $CH_4^{2+} \rightarrow C_mH_n^+ + C_iH_j^+ + N$ (remaining columns)

	a	*b*	H^+	H_2^+	H_3^+
CH_4^+	1320	1320			
CH_3^+	1130	1100	31.2		
CH_2^+	285	236	41.4	7.34	
CH^+	134	110	22.7	0.65	0.08
C^+	52.6	37.5	14.8	0.31	
H_2^+	29.6	17.6	0.59	1.57	
H^+	391	75.9	102		

The electron energy is 200 eV.

$C_2H_5^{2+}$ and $C_2H_3^{2+}$ have been observed in the mass spectrum, they are too weak to be measured accurately. The discrepancy between the present result and our previous measurement [36] is within 8%. Our data have been compared with those of Chatham et al. [50] and Grill et al. [51], which shows that only the cross-sections of $C_2H_n^+$ ($n = 0$–6) from Chatham et al. generally agree with our results [36].

The cross-sections for electron impact ionization and dissociative ionization of propane are listed in column *a* of Table 4. Altogether 22 monocations, namely, $C_3H_n^+$ ($n = 0$–8), $C_2H_n^+$ ($n = 0$–5), CH_n^+ ($n = 0$–3) and H_n^+ ($n = 1$–3) and four dications, namely, $C_3H_n^{2+}$ ($n = 2$–5) have been observed. The charge-weighted total cross-section is 8.43×10^{-16} cm^2, which is only 1% higher than the result of Nishimura and Tawara [43]. The only available partial cross-sections for propane are those from Grill et al. [52]. Their results are generally within ±40% of ours. The experimental setup of Grill et al. strongly discriminates against energetic ions. They measured the kinetic energies of the ions and corrected their data with the calculated collection efficiencies. Their kinetic energy distributions have recently been revised, and for smaller ionic fragments large errors have been found [37], which may significantly affect the correction factors for the cross-sections in their experiment. Since the present experiment measures all the ions directly without discrimination, we believe that our results are more reliable.

The cross-sections for electron impact ionization and dissociative ionization of *n*-butane are listed in column *a* of Table 5. Altogether 32 monocations, namely, $C_4H_n^+$ ($n = 0$–10), $C_3H_n^+$ ($n = 0$–7), $C_2H_n^+$ ($n = 0$–5), CH_n^+ ($n = 0$–3) and H_n^+ ($n = 1$–3) have been observed. The charge-weighted total cross-section is 12.2×10^{-16} cm^2. As has been shown by Nishimura and Tawara [43] and Schram et al. [53], for hydrocarbons at higher electron energies the total cross-sections are approximately proportional to the total number of

Table 3
The cross-sections (10^{-19} cm^2) for electron impact ionization and dissociative ionization of ethane (*a*), for the dissociation channels $C_2H_6^+ \rightarrow C_mH_n^+ + N$ (*b*), and for the dissociation channels $C_2H_6^{2+} \rightarrow C_mH_n^+ + C_iH_j^+ + N$ (remaining columns)

	a	*b*	H^+	H_2^+	H_3^+	C^+	CH^+	CH_2^+	CH_3^+
$C_2H_6^+$	624	624							
$C_2H_5^+$	490	490							
$C_2H_4^+$	1990	1970	8.31	6.42					
$C_2H_3^+$	755	671	45.5	19.7	18.1				
$C_2H_2^+$	504	444	44.7	11.4	3.75				
C_2H^+	104	75.5	26.2	1.97	0.17				
C_2^+	28.1	13.1	14.4	0.49	0.04				
CH_3^+	238	135	2.71	0.30	0.17	0.75	3.69	25.5	34.9
CH_2^+	122	77.5	7.37	0.32	0.10	1.33	3.14	3.22	
CH^+	47.7	28.0	9.46	0.38	0.07	1.24	0.89		
C^+	27.0	13.5	9.35	0.22	0.04	0.29			
H_3^+	31.5	8.12	0.43	0.08	0.18				
H_2^+	76.0	28.1	4.58	1.00					
H^+	435	127	67.7						

The electron energy is 200 eV.

Table 4
The cross-sections (10^{-19} cm^2) for electron impact ionization and dissociative ionization of propane (*a*), for the dissociation channels $C_3H_8^+ \rightarrow C_mH_n^+ + N$ or $C_3H_8^{2+} \rightarrow C_mH_n^{2+} + N$ (*b*), and for the dissociation channels $C_3H_8^{2+} \rightarrow C_mH_n^+ + C_iH_j^+ + N$ or $C_3H_8^{3+} \rightarrow C_mH_n^{2+} + C_iH_j^+ + N$ (remaining columns)

	a	*b*	H^+	H_2^+	H_3^+	C^+	CH^+	CH_2^+	CH_3^+
$C_3H_8^+$	781	781							
$C_3H_7^+$	556	556							
$C_3H_6^+$	134	134							
$C_3H_5^+$	312	308	2.84	0.53	0.62				
$C_3H_4^+$	63.7	59.1	3.01	0.48	1.17				
$C_3H_3^+$	428	372	42.2	5.84	7.02				
$C_3H_2^+$	145	101	35.7	5.46	2.88				
C_3H^+	107	62.1	37.3	5.35	2.27				
C_3^+	24.9	7.79	15.6	1.44	0.10				
$C_2H_5^+$	1810	1800						3.00	8.54
$C_2H_4^+$	1240	1140						7.94	85.2
$C_2H_3^+$	1090	846	24.3	3.24	0.38	2.11	6.16	35.0	168
$C_2H_2^+$	313	191	31.8	3.17	0.31	3.51	8.56	22.4	52.2
C_2H^+	43.3	15.2	15.0	1.21	0.10	1.43	3.12	4.70	2.58
C_2^+	12.4		8.68	0.49	0.04	0.53	0.87	0.87	0.50
$C_3H_5^{2+}$	2.80	2.64	0.12	0.03	0.01				
$C_3H_4^{2+}$	12.0	11.1	0.67	0.14	0.03				
$C_3H_3^{2+}$	6.96	6.14	0.66	0.13	0.03				
$C_3H_2^{2+}$	12.4	10.9	1.27	0.22	0.04				
CH_3^+	515	146	15.3	2.60	0.42	0.54	0.95	2.49	14.8
CH_2^+	151	45.4	18.8	2.26	0.21	0.73	1.69	2.84	
CH^+	53.3	12.9	15.2	1.20	0.10	0.74	0.88		
C^+	29.1	4.30	13.6	0.85	0.07	0.31			
H_3^+	17.8		1.05	0.15					
H_2^+	52.3	6.70	8.59	1.12					
H^+	484		93.6						

The electron energy is 200 eV.

electrons in the molecules. Our total cross-section of *n*-butane is 12% higher than the linear extrapolation of methane, ethane and propane, which is roughly in agreement with this prediction. To our knowledge, there is no available partial cross-section of *n*-butane that can be used to compare with our results. We also measured the relative abundance of the ions at 75 eV electron energy and compared with the results of Fuchs and Taubert [54]. For the major ions $C_3H_n^+$ ($n = 3, 5, 7$), $C_2H_n^+$ ($n = 3$–5) and CH_3^+, their results are within $\pm 10\%$ of ours, whereas for the minor ions the discrepancy increases to $\pm 50\%$.

3.2. Covariance map

As an example of the covariance maps of the alkanes we studied, the covariance map of *n*-butane is shown in Fig. 2. The positions of the mass peaks observed in the single count mass spectrum are also displayed on the bottom and left, which can be used to identify the islands on the map. Since the false coincidences have been subtracted, the counts in the areas such as $C_2H_n^+ + C_4H_j^+$, etc., are very small. Some special traces can be seen on the top-right of the map, which are caused by the metastable decay of *n*-butane monocations and will be discussed later.

One part of the covariance map in Fig. 2 is expanded and displayed in Fig. 3 to show the details, which contains the islands for the dissociation channels $C_4H_{10}^{2+} \rightarrow CH_n^+ + C_3H_j^+ + N$ ($n = 0$–3, $j = 0$–6). The geometrical properties of an island, i.e. the shape, size and orientation, etc., contain useful information for studying the dynamics of the dissociation, such as the kinetic

Table 5
The cross-sections (10^{-19} cm^2) for electron impact ionization and dissociative ionization of *n* -butane (*a*), for the dissociation channels $C_4H_{10}^+ \rightarrow C_mH_n^+ + N$ (*b*), and for the dissociation channels $C_4H_{10}^{2+} \rightarrow C_mH_n^+ + C_iH_j^+ + N$ or $C_4H_{10}^{3+} \rightarrow C_mH_n^{2+} + C_iH_j^+ + N$ (remaining columns)

	a	*b*	H^+	H_2^+	H_3^+	C^+	CH^+	CH_2^+	CH_3^+	C_2^+	C_2H^+	$C_2H_2^+$	$C_2H_3^+$	$C_2H_4^+$	$C_2H_5^+$
$C_4H_{10}^+$	705	705													
$C_4H_9^+$	95.0	95.0													
$C_4H_8^+$	34.0	34.0													
$C_4H_7^+$	38.8	38.8													
$C_4H_6^+$	10.2	10.2													
$C_4H_5^+$	31.9	30.3	1.26	0.16	0.19										
$C_4H_4^+$	12.8	11.1	1.32	0.23	0.14										
$C_4H_3^+$	45.2	34.6	8.73	1.36	0.52										
$C_4H_2^+$	67.5	41.3	21.9	3.47	0.87										
C_4H^+	31.4	16.4	12.6	2.07	0.32										
C_4^+	13.2	8.45	4.09	0.57	0.06										
$C_3H_7^+$	2690	2690													
$C_3H_6^+$	453	437						0.78	15.2						
$C_3H_5^+$	1010	941	3.87					3.54	57.7						
$C_3H_4^+$	92.0	63.6	2.21					1.61	24.6						
$C_3H_3^+$	612	430	24.8	3.28	0.95	1.68	4.39	17.6	129						
$C_3H_2^+$	115	62.1	17.6	2.39	0.44	1.73	3.49	9.48	17.4						
C_3H^+	81.4	28.6	22.2	2.92	0.42	1.59	3.95	8.12	13.6						
C_3^+	14.1	2.53	7.82	0.85	0.07	0.40	0.74	0.89	0.82						
$C_2H_5^+$	1290	1220	3.83					2.11	6.31			4.83	27.6	14.1	7.55
$C_2H_4^+$	1070	906	9.25					2.76	98.4			7.04	28.0	4.63	
$C_2H_3^+$	1550	1170	60.3	14.0	1.66	1.36	3.13	14.8	62.0	0.85	5.60	54.8	53.6		
$C_2H_2^+$	436	232	58.8	9.22	1.16	1.41	3.27	8.56	15.4	1.20	7.03	15.4			
C_2H^+	50.7	11.4	18.3	2.21	0.15	0.58	1.07	1.40	1.14	0.57	0.66				
C_2^+	11.6		7.28	0.69	0.04	0.26	0.41	0.34	0.40	0.07					
$C_3H_5^{2+}$								0.06	0.19						
$C_3H_4^{2+}$							0.06	0.24	0.67						
$C_3H_3^{2+}$							0.05	0.16	0.41						
$C_3H_2^{2+}$							0.08	0.27	0.61						
CH_3^+	760	263	18.4	3.12	1.01	0.83	2.02	8.04	9.68						
CH_2^+	140	34.2	17.4	1.84	0.35	0.99	2.12	1.26							
CH^+	47.8	5.81	14.1	1.38	0.10	0.82	0.38								
C^+	26.2	1.16	11.8	1.15	0.07	0.16									
H_3^+	9.36		0.94	0.19											
H_2^+	67.9		13.1	1.12											
H^+	533		72.8												

The electron energy is 200 eV.

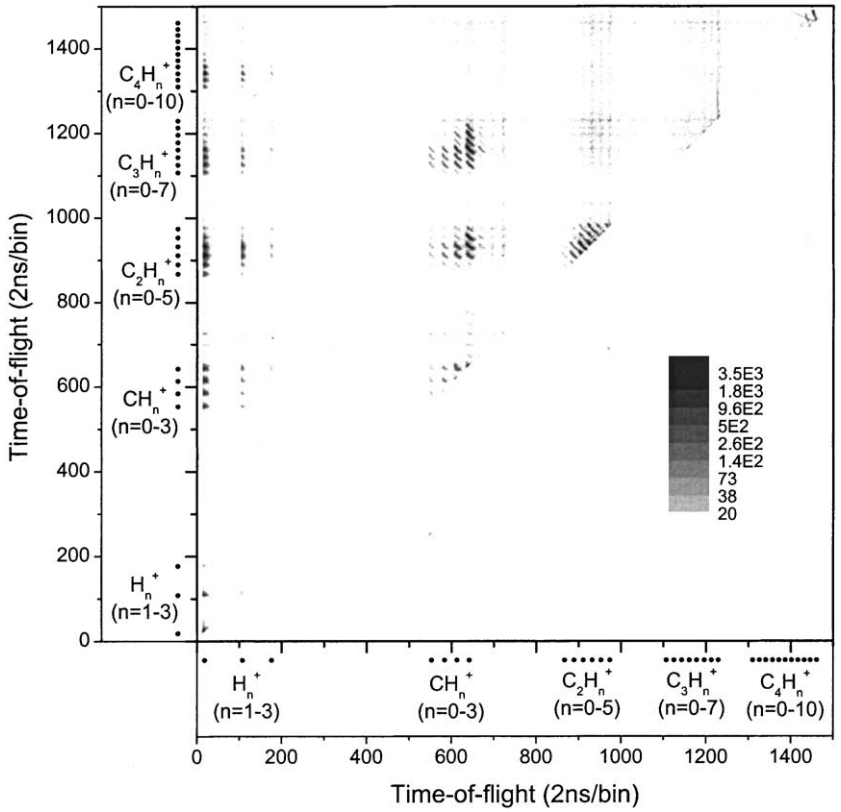

Fig. 2. The covariance map of *n*-butane. The positions of the mass peaks are displayed on the bottom and left.

energy distribution, the directions of the fragments and the dissociation sequence [13,40,55–57]. The theoretical analysis of the covariance mapping mass spectrum has shown that the structure of the island is a momentum contour [40]. The length of the island reflects the kinetic energy of the ion pair, while the width of the island reflects the energy of other undetected fragments. The orientation angle of the island, defined as the angle between the major axis of the island and the x-axis of the map, can be approximated by [40]

$$\theta = \arctan(P_y Q_x / P_x Q_y). \tag{6}$$

Here P and Q are the momentum and charge of the ions displayed on the x- and y-axis. The neutral fragments carry much less momentum than the ionic fragments. This is because the Coulomb repulsion between the two ionic fragments is much stronger than that between one ionic and one neutral fragment. Consequently, the two ionic fragments CH_n^+ and $C_3H_j^+$ have approximately the same momentum but with opposite directions, thus the orientation angle of the island should be close to $-45°$. The orientations of the islands in Fig. 3 support this conclusion. For false coincidence since it happens accidentally, the orientation of the island should always be horizontal or vertical. Therefore obtaining islands with clear orientations other than horizontal and vertical suggests that false coincidence has been efficiently removed from the original total coincidence.

Although the geometrical properties of the islands are very important, all the islands shown in Fig. 3 are a little distorted with respect to normal ellipses. The distortion of the islands may cause much difficulty in interpreting the dissociation dynamics of the molecular ions, thus the origin of

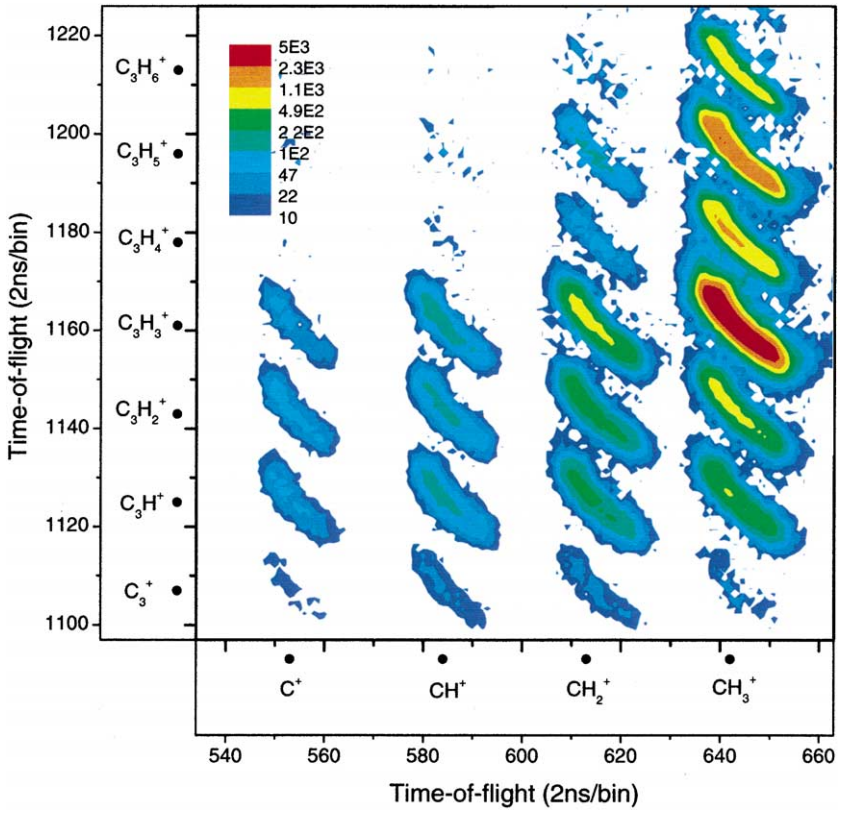

Fig. 3. The covariance map for the dissociation channels $C_4H_{10}^{2+} \rightarrow CH_n^+ + C_3H_j^+ + N$ ($n = 0$–3, $j = 0$–6) in *n*-butane.

the distortion needs to be investigated. The reason for the concave distortion of the islands was supposed by Eland [56] to be the inhomogeneity of the electric field in the mass spectrometer. We found that this supposition is not correct. This can be explained as follows by studying the dependence of the TOF of an ion on its initial momentum. Let the z-axis be the axis of the mass spectrometer, of which the origin is on the extraction mesh. As used by Wiley and McLaren [34], let s be the distance from the ion source to the extraction mesh, d be the length of the acceleration region, and D be the length of the flight tube. Let p be the projection of the initial ion momentum on the z-axis. At first we consider only the case $p \geqslant 0$, i.e. the ion initially flies toward the detector. The TOF of an ion with charge q, mass m is given by

$$t(p,s) = \int_{-s}^{d+D} \frac{m\,\mathrm{d}z}{\sqrt{p^2 + 2mq[V(-s) - V(z)]}}. \tag{7}$$

Here $V(z)$ is the electric potential at the position z. Because the size of the ion beam is much smaller than the ionization region of the spectrometer, we assume that if there is inhomogeneity of the electric field, it is mainly on the z-direction. From Eq. (7) we have

$$\frac{\partial t}{\partial p} = \frac{1}{qV'(-s)}\left(1 - \frac{p}{m}\frac{\partial t}{\partial s}\right). \tag{8}$$

Since in an actual experiment the flight time $t(p,s)$ should have no singular point, using Eq. (8) repeatedly we get

$$\left.\frac{\partial t}{\partial p}\right|_{p=0} = \frac{1}{qV'(-s)}, \tag{9}$$

$$\left.\frac{\partial^2 t}{\partial p^2}\right|_{p=0} = -\frac{1}{mqV'(-s)}\left.\frac{\partial t}{\partial s}\right|_{p=0}, \tag{10}$$

$$\left.\frac{\partial^3 t}{\partial p^3}\right|_{p=0} = -\frac{2V''(-s)}{mq^2[V'(-s)]^3}. \tag{11}$$

For the case $p \leqslant 0$, a turn-around time should be added to Eq. (7). Results show that in this case Eqs. (9)–(11) stay the same. Consequently we have the Taylor series

$$t(p,s) = t_0 - \frac{p}{qE(-s)} + \frac{p^2}{2mqE(-s)}\left.\frac{\partial t}{\partial s}\right|_{p=0} - \frac{E'(-s)p^3}{3mq^2E^3(-s)} + \cdots. \tag{12}$$

Here t_0 is the TOF of the ions with $p = 0$. $E(-s) = -V'(-s)$ is the electric field at the ion source. The second term in Eq. (12), i.e. the linear term, is usually considered as a good approximation. From Eq. (12) it is clear that so far as the dependence of the TOF on the projection of the initial ion momentum is concerned, the status of space focusing, i.e., $(\partial t/\partial s)|_{p=0}$ is responsible for the second-order correction, while the inhomogeneity of the electric field at the ion source, i.e. $E'(-s)$ is responsible for the third-order correction.

In the present experiment the calculation based on the SIMION software gives $E(-s) = 54$ V/mm and $E'(-s) = 3.7$ V/mm^2 for the FTOF spectrometer. Using these values, we find that for monocations with an initial energy of 10 eV the third-order correction is less than 2% of the linear term. Therefore in our experiment, the distortion of the islands is mainly caused by the deviation from the space focusing condition $(\partial t/\partial s)|_{p=0} = 0$. This is in agreement with the shapes of the islands in Fig. 3. The two ends of the islands have been turned into the same direction, here against the origin of the map plane. Since the second-order correction in Eq. (12) is proportional to $m^{-1/2}$, the distortion is stronger for lighter ions, as can be seen later. The difficulty in achieving the space focusing condition is caused by the finite spatial size of the interaction region, the temporal width of the electron beam and the delay between the electron beam and the extraction pulse. Distortions of the islands caused by the deviation from the space focusing condition can also be seen in other experiments [27,40,56], in which concavities of the islands can be seen. On the other hand, the distortion of the islands caused by the inhomogeneity of the electric field can also be seen in some experiments [6,57,58], where the two ends of the island are turned into opposite directions.

3.3. Cross-sections for the different dissociation channels

3.3.1. Methane

The cross-sections for the dissociation of methane monocations, i.e. $\sigma_1(m,n)$ for $CH_4^+ \rightarrow C_mH_n^+ + N$ are listed in column b of Table 2. The total cross-section of single ionization, by summing up $\sigma_1(m,n)$, is 2.89×10^{-16} cm^2. About 46% of the methane monocations stabilize into CH_4^+, and the others will dissociate. The cross-section for $CH_4^+ \rightarrow CH_n^+ + N$ $(n = 0$–$3)$ decreases nearly exponentially when n decreases, among which $CH_4^+ \rightarrow CH_3^+ + H$ is dominant and accounts for 70% of the dissociative CH_4^+ ions. The dissociation into H_n^+ $(n = 1, 2)$ contributes only 6% to the dissociative CH_4^+ ions.

The dissociation of CH_4^+ has been studied by Kupriyanov and Perov [25] through collision with air and deuterium, and by Ben-Itzhak et al. [6] through proton impact at 4 MeV. So far as the relative abundance of the ionic fragments is concerned, the result of Kupriyanov and Perov at 3.5 keV ion energy, and the result of Ben-Itzhak et al. have generally a similar tendency as ours. An overall good agreement between these experiments is not expected since the excitation methods and the excitation energies used in these experiments are very different.

The cross-sections for the dissociation of methane dications, i.e. $\sigma_2(m,n,i,j)$ for CH_4^{2+} *arrow*$C_mH_n^+ + C_iH_j^+ + N$, are listed in the remaining columns of Table 2. The total double ionization of methane, calculated by summing up $\sigma_2(m,n,i,j)$, is 0.223×10^{-16} cm^2, which is 8% of the total single ionization. It is notable that although no H_3^+ ion can be clearly observed in the single count spectrum, the dissociation channel $CH_4^{2+} \rightarrow CH^+ + H_3^+$ has been observed on the

covariance map. The top three abundant dissociation channels, and their contributions to the dissociation of CH_4^{2+} are $CH_4^{2+} \rightarrow 2H^+ + N$ (46%), $CH_4^{2+} \rightarrow H^+ + CH_2^+ + H$ (19%) and $CH_4^{2+} \rightarrow H^+ + CH_3^+$ (14%).

The dissociation of CH_4^{2+} has been studied by Ben-Itzhak et al. [6] through proton impact at 4 MeV, by Backx and Van der Wiel [29] through electron impact at 10 keV, by McCulloh et al. [30] through electron impact at 1 keV and by Fournier et al. [26] through HeII photoionization. For the dissociation channels $CH_4^{2+} \rightarrow H_j^+ + CH_n^+ + N$ $(n + j \leqslant 4)$, the results from Ben-Itzhak et al. and from Backx and Van der Wiel have a similar distribution pattern as ours. The discrepancy between each other is in general within ±30%. The early data of McCulloh et al. are much smaller than those of other authors. This may be caused by the failure of collecting the energetic ions. The fragmentation pattern of Fournier et al. is different from others since the energy used in their experiment is much smaller. It is remarkable that although $CH_4^{2+} \rightarrow 2H^+ + N$ in our experiment is found to be the most abundant channel, it was not reported as a significant channel in all the previous experiments. This is because in those experiments all the ion pairs that come very closely are lost due to the long dead time of the detection electronics.

3.3.2. Ethane

The cross-sections for the dissociation of ethane monocations, i.e. $\sigma_1(m,n)$ for $C_2H_6^+ \rightarrow C_mH_n^+ + N$ are listed in column *b* of Table 3. The total cross-section of single ionization, by summing up $\sigma_1(m,n)$, is 4.71×10^{-16} cm^2. Only 13% of the $C_2H_6^+$ ions are stable, and the others will dissociate. The most abundant dissociation channel is $C_2H_6^+ \rightarrow C_2H_4^+ + H_2$ (or 2H), which accounts for 48% of the dissociative $C_2H_6^+$ ions. The cross-section for $C_2H_6^+ \rightarrow CH_n^+ + N$ $(n = 0–3)$ decreases nearly exponentially when n decreases. The dissociation into H_n^+ $(n = 1–3)$ accounts for only 4% of the dissociative $C_2H_6^+$ ions.

Since no dications are clearly observed in the single count spectrum, all the ethane dications are assumed to dissociate through $C_2H_6^{2+} \rightarrow C_mH_n^+ + C_iH_j^+ + N$. Their cross-sections, i.e. $\sigma_2(m,n,i,j)$ are listed in the remaining columns of Table 3. The total double ionization cross-section, calculated by summing up $\sigma_2(m,n,i,j)$, is 0.381×10^{-16} cm^2, which is 8% of the total single ionization. The top three abundant dissociation channels, and their contributions to the dissociation of $C_2H_6^{2+}$ are $C_2H_6^{2+} \rightarrow 2H^+ + N$ (18%), $C_2H_6^{2+} \rightarrow H^+ + C_2H_3^+ + N$ (12%) and $C_2H_6^{2+} \rightarrow H^+ + C_2H_2^+ + N$ (12%).

3.3.3. Propane

The cross-sections for the dissociation channels $C_3H_8^+ \rightarrow C_mH_n^+ + N$, i.e. $\sigma_1(m,n)$ are listed in column *b* of Table 4. Here the cross-sections for $C_2^+ + N$ and $H_n^+ + N$ $(n = 1, 3)$ are not shown, because if we use Eq. (4) the cross-sections for these channels are found to be less than 5% of $\sigma^+(m,n)$ shown in column *a*. This simply means that the dissociation of $C_3H_8^+$ contributes very little to these ions, and they cannot be accurately measured through the present method. The total cross-section of single ionization, by summing up $\sigma_1(m,n)$, is 6.56×10^{-16} cm^2. Only 12% of the $C_3H_8^+$ ions are stable, the remaining ions will dissociate. The top two abundant dissociation channels are $C_3H_8^+ \rightarrow C_2H_5^+ + N$ and $C_3H_8^+ \rightarrow C_2H_4^+ + N$, which account for 51% of the dissociative $C_3H_8^+$ ions. This indicates that $C_3H_8^+$ is easy to eliminate a methyl radical directly, or eliminate a methane molecule after rearrangement of the hydrogen atoms. Among all the channels $C_3H_8^+ \rightarrow C_3H_n^+ + N$ of the dissociative $C_3H_8^+$ ions, $n = 7, 5, 3$ are the dominant pathways. The cross-section for $C_3H_8^+ \rightarrow C_2H_n^+ + N$ $(n = 0–5)$ decreases monotonically when n decreases. The cross-section for $C_3H_8^+ \rightarrow CH_n^+ + N$ $(n = 0–3)$ decreases nearly exponentially when n decreases.

Kupriyanov and Perov [24] have measured the cross-sections for $C_3H_n^+$ $(n = 1–7)$, $C_2H_n^+$ $(n = 1–5)$ and CH_n^+ $(n = 0–3)$ from the dissociation of propane monocations due to collision with neon atoms at 3.5 keV energy. The relative abundances of the ionic fragments obtained by them have a very similar behavior as ours. This suggests that at the ion energy they used, after collision with neon $C_3H_8^+$ ions may have a similar excitation distribution as that in our experiment.

The cross-sections for the dissociation channels $C_3H_8^{2+} \rightarrow C_mH_n^{2+} + N$, i.e. $\sigma_2(m,n)$ are also listed in column *b* of Table 4. The cross-sections for

$C_3H_8^{2+} \rightarrow C_mH_n^+ + C_iH_j^+ + N$, i.e. $\sigma_2(m,n,i,j)$ are listed in the remaining columns. The total cross section of double ionization, by summing up $\sigma_2(m,n)$ and $\sigma_2(m,n,i,j)$, is 0.908×10^{-16} cm^2. In the dissociation channels $C_3H_8^{2+} \rightarrow C_mH_n^{2+} + N$, only four channels, $C_3H_8^{2+} \rightarrow C_3H_n^{2+} + N$ ($n = 2$–5) have been observed. They contribute only 3% to the dissociation of $C_3H_8^{2+}$. The ion-pair dissociation channels, i.e. $C_3H_8^{2+} \rightarrow C_mH_n^+ + C_iH_j^+ + N$ are the dominant pathways. The top three abundant dissociation channels, and their contributions to the dissociation of $C_3H_8^{2+}$ are $C_3H_8^{2+} \rightarrow CH_3^+ + C_2H_3^+ + N$ (19%), $C_3H_8^{2+} \rightarrow 2H^+ + N$ (10%) and $C_3H_8^{2+} \rightarrow CH_3^+ + C_2H_4^+ + N$ (9%).

Among the dissociation of propane trications, only the cross-sections for $C_3H_8^{3+} \rightarrow H_n^+ + C_3H_j^{2+} + N$ ($n = 1$–3, $j = 2$–5) are measured and listed in Table 4. The total cross-section of triple ionization, from the measured channels, is only 0.0033 $\times 10^{-16}$ cm^2, which is more than two orders of magnitude smaller than double ionization. As can be seen in Table 4, the dissociation of $C_3H_8^{2+}$ contributes a major part of the $C_3H_n^{2+}(n = 2$–$5)$ ions, while the dissociation of $C_3H_8^{3+}$ contributes only a little. This can be confirmed by observing the shape of the mass peaks of $C_3H_n^{2+}$ ($n = 2$–5) in Fig. 1(c). Since these ions come mostly from the dissociation of dications, they have small initial kinetic energies and thus can be well resolved. Due to Coulomb explosion $C_3H_8^{3+}$ ions tend to dissociate into the smallest possible ionic fragments, hence in the measured channels $C_3H_8^{3+} \rightarrow H^+ + C_3H_2^{2+} + N$ is the largest and $C_3H_8^{3+} \rightarrow H_3^+ + C_3H_5^{2+}$ is the smallest.

3.3.4. n-Butane

The cross-sections for the dissociation of *n*-butane monocations, i.e. $\sigma_1(m,n)$ for $C_4H_{10}^+ \rightarrow C_mH_n^+ + N$ are listed in column *b* of Table 5. The cross sections for $C_2^+ + N$ and $H_n^+ + N$ ($n = 1$–3) are not shown because of their small values comparing to the uncertainty of our experimental method. The total cross-section of single ionization, by summing up $\sigma_1(m,n)$, is 9.52×10^{-16} cm^2. Only 7% of the *n*-butane monocations is stable, others will dissociate. The top two abundant dissociation channels are $C_4H_{10}^+ \rightarrow C_3H_7^+ + N$ and $C_4H_{10}^+ \rightarrow C_2H_5^+ + N$, in which the former channel is about twice as abundant as the latter. They contribute 44% to the dissociative $C_4H_{10}^+$ ions. This indicates that $C_4H_{10}^+$ ions are easy to dissociate by simply breaking one side or center C–C bond with approximately the same probability. Again the cross-section for $C_4H_{10}^+ \rightarrow CH_n^+ + N$ ($n = 0$–3) decreases nearly exponentially when n decreases. The elimination of neutral hydrogen, i.e. $C_4H_{10}^+ \rightarrow C_4H_n^+ + N$ ($n = 0$–9) is very small and contributes only 4% to the dissociative $C_4H_{10}^+$ ions. This is different from ethane and propane monocations, indicating that larger alkane monocations have a tendency to break more C–C bonds and produce smaller fragments.

All the *n*-butane dications are found to dissociate through $C_4H_{10}^{2+} \rightarrow C_mH_n^+ + C_iH_j^+ + N$, the corresponding cross-sections $\sigma_2(m,n,i,j)$ are listed in the remaining columns of Table 5. The total cross-section of double ionization, by summing up $\sigma_2(m,n,i,j)$, is 1.30×10^{-16} cm^2. The top three abundant dissociation channels, and their contributions to the dissociation of $C_4H_{10}^{2+}$ are $C_4H_{10}^{2+}$ *arrow*$CH_3^+ + C_3H_3^+ + N$ (10%), $C_4H_{10}^{2+} \rightarrow CH_3^+ + C_2H_4^+ + N$ (8%) and $C_4H_{10}^{2+} \rightarrow 2H^+ + N$ (6%).

Although no dication can be clearly observed in the single count spectrum, some minor dissociation channels of *n*-butane trications through $C_4H_{10}^{3+} \rightarrow C\ H_n^+ + C_3H_j^{2+} + N$ ($n = 1$–3, $j = 2$–5) are observed on the covariance map and also listed in Table 5. The total cross-section of triple ionization calculated from these channels is only 0.0028×10^{-16} cm^2. It is more than two orders of magnitude smaller than double ionization.

3.4. Comparison with the BEB model

In recent years, there has been much progress in the theoretical calculation of the absolute total electron impact ionization cross sections of molecules (for a recent review see [59]), among which the Deutsch–Märk (DM) formalism [59,60] and the binary-encounter-Bethe (BEB) formalism [61] have been widely used. Both methods use the quantum mechanically determined molecular parameters and sum up the ionization cross-section for each molecular orbital. At around 200 eV the results of these two methods for methane [59], ethane [59] and propane [62] agree well with each other. We have compared our cross-sections with

Table 6
Total electron impact ionization cross-sections (10^{-19} cm^2) calculated by the BEB method (*a*), total single (*b*), double (*c*) and triple (*d*) ionization cross-sections (10^{-19} cm^2) from the present experiment

Molecule	*a*	*b*	*c*	*d*
CH_4	2.682	2.89	0.233	
C_2H_6	4.854	4.71	0.381	
C_3H_8	6.624	6.56	0.908	0.0033
C_4H_{10}	9.343	9.52	1.30	0.0028

Note that column *d* is only from the measured channels (see text). The electron energy is 200 eV.

those calculated from the BEB method. The required molecular constants for methane [63], ethane [61] and propane [61] are taken from the literature. The molecular parameters for *n*-butane are obtained from Irikura and Kim through private communications.

The total cross-sections calculated from the BEB method are listed in Table 6, together with our experimental total cross-sections for single ionization (by summing up $\sigma_1(m,n)$), double ionization (by summing up $\sigma_2(m,n)$ and $\sigma_2(m,n,i,j)$) and triple ionization. Note that the total triple ionization cross-sections are only from the measured channels. The agreement between the total BEB cross-sections and our total single ionization cross-sections is satisfactory, the discrepancy is 8% for methane and within 3% for other molecules. The double ionizations cannot be included in the DM and BEB formalisms. In order to compare the BEB cross-sections directly with the experiments that measure the total ion number or ion current, Kim and Rudd [64] assumed that the double ionizations originate from Auger processes and can be included by simply doubling the cross sections for those inner-shell orbitals whose binding energies are greater than the double ionization threshold of the molecule. This may not work for many molecules. One reason is that the actual double ionization threshold may be much lower than the binding energy of the orbital from which the cross-section is begin to be doubled. Also the contributions from triple and quadruple ionization may not be negligible at higher electron energies. As has been done in the present study, a better way of testing the DM and BEB theory is to compare them with the experiments in which the actual single ionization cross-section has been obtained through coincidence techniques.

3.5. Small dissociation channels

As shown above, the dissociation channel $CH_4^{2+} \rightarrow CH^+ + H_3^+$ has been observed on the covariance map of methane although no H_3^+ ion can be clearly seen in the single count spectrum. Actually no H_3^+ ion has been reported in electron impact ionization of methane. The covariance map of this channel is shown in Fig. 4(a). The distortion of this island has been explained above as due to the devi-

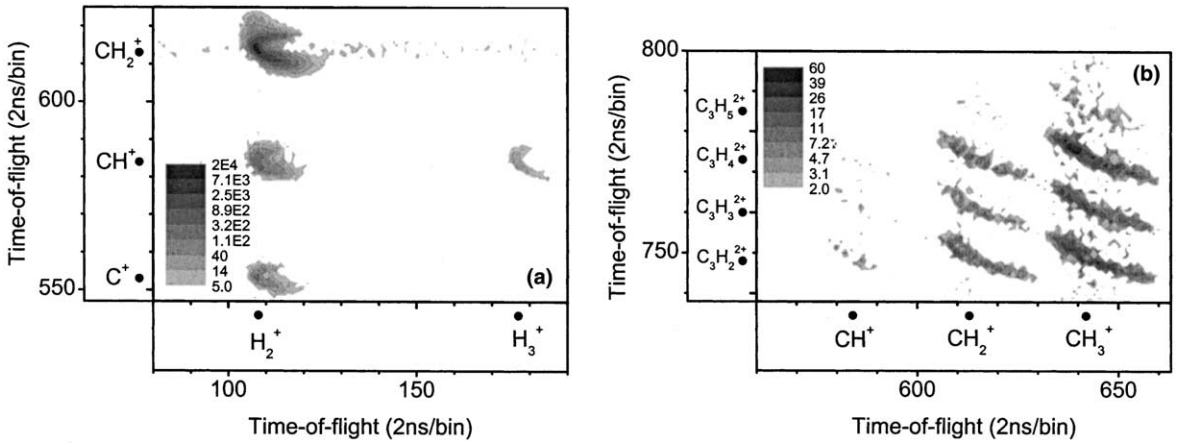

Fig. 4. Small dissociation channels observed in: (a) methane, $CH_4^{2+} \rightarrow CH^+ + H_3^+$; (b) *n*-butane, $C_4H_{10}^{3+} \rightarrow CH_n^+ + C_3H_j^{2+} + N$ ($n = 1$–3, $j = 2$–5).

ation from the space focusing condition. The H_3^+ ion is light, the masses between CH^+ and H_3^+ are quite different, and they also have a large initial momentum. According to Eq. (12) at larger initial momentum the shape of this island will change from $x = -y$ into $x \propto y^2$, where x and y are the TOF of the two ions measured from the center of the island. This feature can be seen in Fig. 4(a). Siegbahn [65] has suggested theoretically that for the dissociation of CH_4^{2+} the simultaneous breaking of three C–H bonds and resulting in $CH^+ + H_3^+$ is much less likely, because the dissociation dynamics favors the breaking of fewer C–H bonds. Our result shows that the abundance of $CH_4^{2+} \rightarrow CH^+ + H_3^+$ is only about 0.3% of $CH_4^{2+} \rightarrow CH_3^+ + H^+$.

In *n*-butane although no dication has been clearly seen in the single count spectrum, the dissociation channels $C_4H_{10}^{3+} \rightarrow CH_n^+ + C_3H_j^{2+} + N$ ($n = 1$–3, $j = 2$–5) are observed on the covariance map. They are shown in Fig. 4(b). The orientation of the islands has an average angle of $26 \pm 2°$, which agrees well with Eq. (6), i.e. $\arctan(1/2) = 26.6°$. As shown in Table 5, the abundance of these channels is more than two orders of magnitude smaller than the major ion-pair dissociation channels.

Observing very weak dissociation channels, of which the minor ionic products cannot be seen in the single count spectrum, indicates that the covariance mapping technique has a high sensitivity. This is because the covariance map has decomposed the mass peaks in the single count spectrum into different dissociation channels. The minor ions immersed in the large background in the single count spectrum have been displayed in the covariance map with a new circumstance where the background noise has been significantly reduced.

3.6. Ionic product distribution from the dissociation of alkane dications

We have calculated the distribution of the total ionic products on different ionic species from the dissociation of alkane dications. The results are shown in Fig. 5, which can be considered as the projection of all the corresponding islands onto one axis of the covariance map. Since dication fragments are minor species they are not shown here. The similarities between the four alkanes are

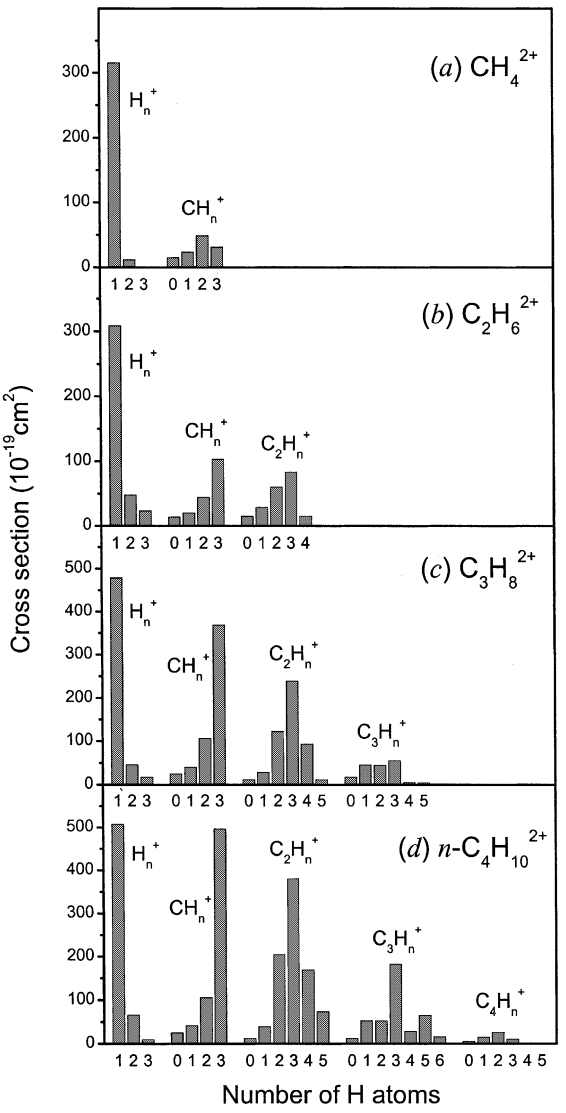

Fig. 5. Ionic product distribution from the dissociation of alkane dications: (a) methane; (b) ethane; (c) propane; (d) *n*-butane.

apparent. Protons are the most abundant products for all these alkane dications. This is not surprising since protons are produced from many dissociation channels, and proton pairs are among the first few abundant channels for the dissociation of alkane dications. For ethane, propane and *n*-butane dications, the second, third and fourth abundant ion species are all found to be CH_3^+, $C_2H_3^+$ and $C_2H_2^+$, respectively. Even the sequences of the less abundant ionic species from ethane, propane and

n-butane dications show clear similarities. For example, H_n^+ ($n = 1$–3) decreases when n increases, CH_n^+ ($n = 0$–3) increases when n increases, and $C_2H_n^+$ ($n = 0$–5) has a single maximum at $n = 3$. These similarities indicate that the properties of the final products, e.g. the internal energies, the stabilities etc. play an important role in the dissociation of molecular ions.

3.7. Metastable decays

In our experiment there appear some weak traces on the covariance maps. An example of these traces is shown in Fig. 6(a) from the covariance map of propane. This trace starts from the island $CH_3^+ + C_2H_2^+$ and ends on the diagonal at the time bin of $C_3H_5^{2+}$. These special structures are formed by the decay of metastable parent ions that have lifetimes comparable to the TOF scale in the experiment. Similar traces have been observed by Field and Eland [66] in the dissociation of CO^{2+}, and by Besnard-Ramage et al. [67] in the dissociation of $C_6F_6^{2+}$. A metastable decay trace usually starts from a certain island and ends at a certain point on the diagonal. It is easy to identify the trace shown in Fig. 6(a) as $C_3H_5^{2+} \rightarrow CH_3^+ + C_2H_2^+$. However, for metastable ions with shorter lifetimes, the end of the decay trace may not be visible. In this case the parent ion cannot be simply considered as the sum of the daughter ions, because a third fragment is also possible to exist. On the other hand, if the metastable ions have a longer lifetime, the start of the decay trace may not be visible. We have found that the initial and final angles of a decay trace, defined as the tilting angles of the initial and final parts of the trace with respect to the x-axis, are useful in identifying the trace.

The initial angle of a metastable decay trace can be calculated as follows. Since the initial energies of the parent ions are negligible compared to the energy gained in the mass spectrometer, we consider only the parent ions that have no momentum projection on the z-axis of the spectrometer. Also we consider only the daughter ions that have no additional momentum projection due to the dissociation. These ions form the center curve of the decay trace. Let m, m_1, m_2, q, q_1 and q_2 be the masses and charges of the parent ion, the first daughter ion and the second daughter ion, respectively. Suppose the parent ion dissociates at the position z_0, the TOF of the first daughter ion is described by

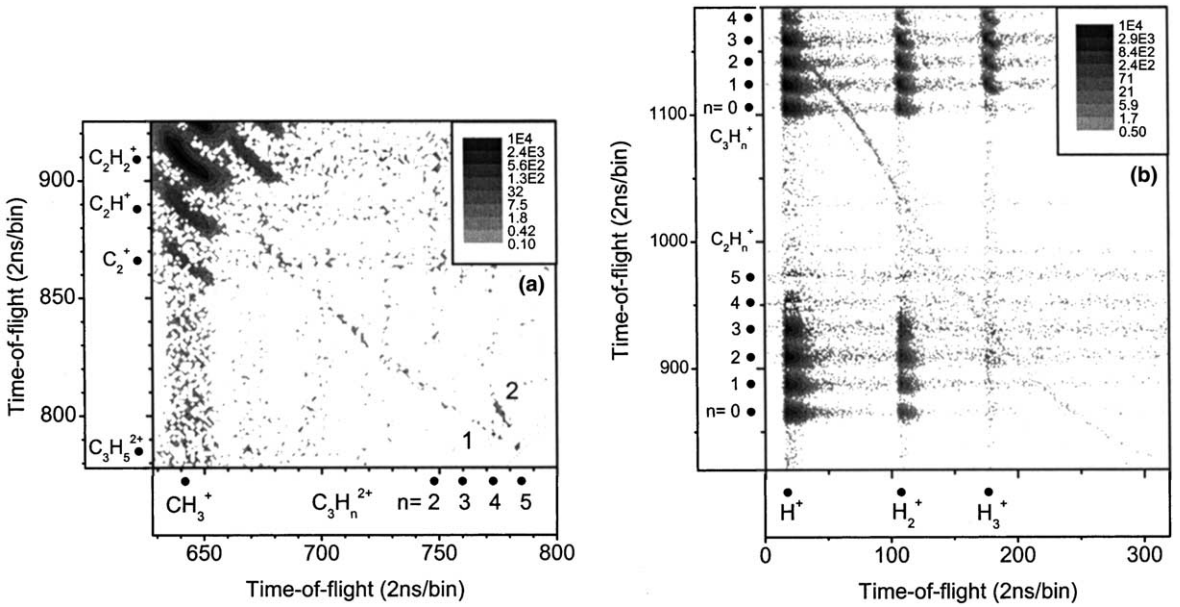

Fig. 6. Metastable decay traces observed in propane: (a) $C_3H_5^{2+} \rightarrow CH_3^+ + C_2H_2^+$; (b) $C_3H_4^{2+} \rightarrow H^+ + C_3H_3^+$.

$$t_1 = \int_{-s}^{z_0} \left(m\,\mathrm{d}z \Big/ \left(\sqrt{2mq[V(-s) - V(z)]} \right) \right) + \int_{z_0}^{d+D} \left(m\,\mathrm{d}z \Big/ \left(\sqrt{2mq[V(-s) - V(z_0)] + (2m^2/m_1)q_1[V(z_0) - V(z)]} \right) \right). \tag{13}$$

A similar equation can be written for the second daughter ion. Let θ be the initial angle of the decay trace, we have

$$\tan\theta = \lim_{z_0 \to -s} \left(\frac{\partial t_2}{\partial z_0} \Big/ \frac{\partial t_1}{\partial z_0} \right) = \frac{q_1}{q_2} \left(\frac{mq_2 - m_2 q}{mq_1 - m_1 q} \right). \tag{14}$$

For a two-body ion-pair separation of dications, i.e. $q = 2, q_1 = q_2 = 1$ and $m = m_1 + m_2$, this simply results in an initial angle of $\theta = -45°$.

The final angle of a metastable decay trace can be calculated as follows. Since the electric field in the flight tube is very week, the momenta of the daughter ions gained from the dissociation must be considered when calculating the difference of the TOF between the ions. Let p_1 and p_2 be the momentum projections of the daughter ions obtained in the dissociation in the center-of-mass frame. Suppose the parent ion dissociates at the position z_0 in the flight tube. Let t_0 be the TOF of the parent ion if it does not dissociate, and P be the momentum projection of the parent ion. If we neglect the electric field in the flight tube, the TOF of the first daughter ion is

$$t_1 = t_0 + (d + D - z_0)\left[\frac{1}{(P/m) + (p_1/m_1)} - \frac{1}{P/m} \right] = t_0 - \frac{d + D - z_0}{(P/m)^2} \frac{p_1}{m_1}. \tag{15}$$

A similar equation for the second daughter ion can also be written. For a two-body separation, we have $p_1 = -p_2$. If $p_1 > 0$, the first ion is faster, let θ_1 be the final angle of the decay trace, we have

$$\tan\theta_1 = -m_2/m_1. \tag{16}$$

If $p_1 < 0$, the second ion is faster, let θ_2 be the final angle of the decay trace, we have

$$\tan\theta_2 = -m_1/m_2. \tag{17}$$

As a result two linear branches, which form a V-shape, appear at the end of the decay trace. This can be seen in Fig. 6(a). Similar V-shape decay traces have been observed by other authors [13,66]. For a metastable decay that has more than two fragments, it is very likely that p_1, p_2 and p_3, etc., are proportional to each other [40]. In this case more than one V-shape should originate from the same point on the diagonal of the covariance map.

The metastable decay traces observed in propane are shown in Fig. 6, and those observed in *n*-butane are shown in Fig. 7. All the clearly observed decay traces in ethane, propane and *n*-butane have been identified as listed in Table 7. Also shown are the islands from which the traces start, the points at which the traces end, and the measured initial and final angles. The metastable decays $C_2H_4^{2+} \rightarrow H^+ + C_2H_3^+$ in ethane, and $C_3H_4^{2+} \rightarrow H^+ + C_3H_3^+$ in propane have been observed by Hagan and Eland [8]. All the decay traces have an initial angle near −45°, or have only one V-shape originating from the diagonal, this means that they are two-body separations.

In the covariance map of *n*-butane, two V-shapes originating from the diagonal at the time bins of $C_4H_{10}^+$ and $C_4H_9^+$, respectively, have been observed as shown in Fig. 7(b). Because in our experiment the backing pressure is only on the order of 1 Torr, no dimer can be formed in the effusive flow through the long needle. The parent ions should be considered as $C_4H_{10}^+$ and $C_4H_9^+$, and the two V-shapes can be interpreted as each parent ion decays into one ionic and one neutral fragment. Because these decays occur in the flight tube, the neutrals have gained enough energy to trigger the detector [68]. Since Eq. (15) also applies to neutrals, Eqs. (16) and (17) can be used to determine the species of the fragments. These metastable decays are identified as the elimination of methyl radicals from the parent ions, i.e.

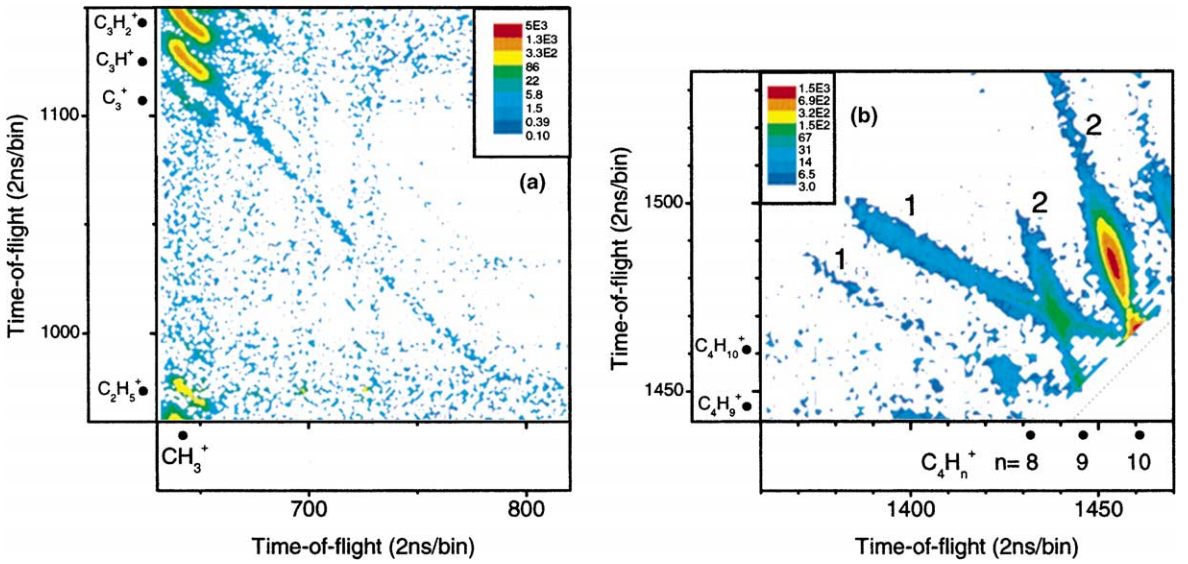

Fig. 7. Metastable decay traces observed in *n*-butane: (a) $C_4H_4^{2+} \rightarrow C_3H^+ + CH_3^+$; (b) $C_4H_{10}^+ \rightarrow C_3H_7^+ + CH_3$ and $C_4H_9^+ \rightarrow C_3H_6^+ + CH_3$.

Table 7
The metastable decay traces observed in electron impact dissociative ionization of ethane, propane and *n*-butane

Molecule	Start	End	θ	θ_1	θ_2	Identification
C_2H_6	$H^+ + C_2H_3^+$		$-46.1 \pm 1.5°$			$C_2H_4^{2+} \rightarrow H^+ + C_2H_3^+$
C_3H_8	$CH_3^+ + C_2H_2^+$	$C_3H_5^{2+}$	$-45.7 \pm 1.5°$	$-29.7 \pm 1.5°$	-60.6 ± 1	$C_3H_5^{2+} \rightarrow CH_3^+ + C_2H_2^+$
	$H^+ + C_3H_3^+$		$-45.9 \pm 1.5°$			$C_3H_4^{2+} \rightarrow H^+ + C_3H_3^+$
C_4H_{10}	$CH_3^+ + C_3H^+$		$-45.5 \pm 1°$			$C_4H_4^{2+} \rightarrow CH_3^+ + C_3H^+$
		$C_4H_{10}^+$		$-19.6 \pm 1.5°$	$-71.3 \pm 1°$	$C_4H_{10}^+ \rightarrow C_3H_7^+ + CH_3$
		$C_4H_9^+$		$-20.6 \pm 2°$	$-70.8 \pm 1°$	$C_4H_9^+ \rightarrow C_3H_6^+ + CH_3$

The angles θ, θ_1 and θ_2 are the initial angle and the two final angles between the decay trace and the *x*-axis of the covariance map.

$C_4H_{10}^+ \rightarrow C_3H_7^+ + CH_3$ and $C_4H_9^+ \rightarrow C_3H_6^+ + CH_3$. The intensity of the decay $C_4H_{10}^+ \rightarrow C_3H_7^+ + CH_3$ is very strong, it even affects the resolvability of its neighbor mass peaks in the single count spectrum, as can be seen in Fig. 1(d). It is notable that for the decay trace $C_4H_{10}^+ \rightarrow C_3H_7^+ + CH_3$ the intensities of the two branches are significantly asymmetric, branch 2 is more than one order of magnitude stronger than branch 1. A similar contrast can also be seen in the decay $C_4H_9^+ \rightarrow C_3H_6^+ + CH_3$. This asymmetry indicates that the parent ions have been highly oriented before they dissociate. Since branch 2 is more intense, the heavier fragment, i.e. $C_3H_7^+$ or $C_3H_6^+$, tends to arrive earlier at the detector. This implies that the parent ion is asymmetrically charged, during the acceleration the charged part of the parent ion has been aligned toward the detector.

4. Conclusions

We have studied the dissociation of up to triply ionized methane, ethane, propane and *n*-butane through electron impact ionization at an electron energy of 200 eV. A covariance mapping technique is used to record the ionic fragments in double coincidence and decompose the ionic products into various dissociation channels. A focusing time-of-flight mass spectrometer is used

to collect all the ions without initial kinetic energy discrimination. Electron impact ionization and dissociative ionization cross-sections of these alkanes are measured. The dissociation channels of the alkane monocations, dications and trications are identified. The absolute cross-sections for numerous ion-pair dissociation channels of all the alkane dications as well as propane and *n*-butane trications have been measured from the counts of the corresponding islands on the covariance maps. The cross sections for the dissociation channels that have only one ionic product are derived.

All the alkane dications are unstable and most of them dissociate through ion-pair dissociation channels, of which the production of proton pairs is found to be a considerable major dissociation channel. The total single ionization cross-sections agree well with the total cross-sections calculated from the BEB method. Very small dissociation channels such as $CH_4^{2+} \rightarrow CH^+ + H_3^+$ in methane and $C_4H_{10}^{3+} \rightarrow CH_n^+ + C_3H_j^{2+} + N$ ($n = 1$–3, $j = 2$–5) in *n*-butane have been observed on the covariance maps, although the minor ionic fragments H_3^+ and $C_3H_j^{2+}$ cannot be seen in the corresponding single count spectra. The ionic product distributions from the dissociation of ethane, propane and *n*-butane dications are found to be similar, of which the first few abundant ion species are $H^+, CH_3^+, C_2H_3^+$ and $C_2H_2^+$.

The reason for the distortion of the shapes of the ion coincidence islands has been investigated. The concavity of the islands is explained as due to the deviation from the space focusing condition of the mass spectrometer. Some metastable decay traces have been observed and identified in the covariance maps. The initial and final angles of the decay traces are found to be useful in determining the origins of these traces. Special decay traces, in which neutrals are produced, such as the elimination of methyl radicals from *n*-butane monocations have also been observed.

Acknowledgements

One of the authors (P. Wang) is grateful to the Alexander von Humboldt Foundation for providing the financial support for staying at the Max-Planck Institute for Extraterrestrial Physics. We thank Dr. K.K. Irikura and Dr. Y.-K. Kim for calculating the molecular parameters of *n*-butane. The technical assistance from Bernd Steffes and the helpful discussions with Cechan Tian are also appreciated.

References

[1] D. Mathur, Phys. Rep. 225 (1993) 193.
[2] D. Schröder, H. Schwarz, J. Phys. Chem. A 103 (1999) 7385.
[3] M. Larsson, Comments At. Mol. Phys. 29 (1993) 39.
[4] B. Siegmann, U. Werner, H.O. Lutz, Aust. J. Phys. 52 (1999) 545.
[5] U. Werner, J. Becker, T. Farr, H.O. Lutz, Nucl. Instrum. Meth. B 124 (1997) 298.
[6] I. Ben-Itzhak, K.D. Carnes, S.G. Ginther, D.T. Johnson, P.J. Norris, O.L. Weaver, Phys. Rev. A 47 (1993) 3748.
[7] A.K. Shukla, K. Qian, S.G. Anderson, J.H. Futrell, Int. J. Mass Spectrom. Ion Process. 109 (1991) 227.
[8] D.A. Hagan, J.H.D. Eland, Org. Mass Spectrom. 27 (1992) 855.
[9] Ph. Hering, C. Cornaggia, Phys. Rev. A 59 (1999) 2836.
[10] K. Codling, L.J. Frasinski, J. Phys. B 26 (1993) 783.
[11] S. Banerjee, G.R. Kumar, D. Mathur, Phys. Rev A 60 (1999) R25.
[12] F. Scheuermann, E. Salzborn, F. Hagelberg, P. Scheier, J. Chem. Phys. 114 (2001) 9875.
[13] C. Tian, C.R. Vidal, Phys. Rev. A 58 (1998) 3783.
[14] C. Tian, C.R. Vidal, Phys. Rev. A 59 (1999) 1955.
[15] K.H. Becher, V. Tarnovsky, Plasma Sourc. Sci. Technol. 4 (1995) 307.
[16] T.D. Märk, G.H. Dunn, Electron impact ionization, Springer-Verlag, Wien, 1985.
[17] W.M. Huo, Y.-K. Kim, IEEE Trans. Plasma Sci. 27 (1999) 1225.
[18] E. Meeks, P. Ho, Thin Solid Films 365 (2000) 334.
[19] H.M. Rosenstock, M.B. Wallenstein, A.L. Wahrhaftig, H. Eying, Proc. Natl. Acad. Sci. USA 38 (1952) 667.
[20] J.C. Schug, J. Chem. Phys. 38 (1962) 2610.
[21] S. Meyerson, J. Chem. Phys. 42 (1965) 2181.
[22] M.L. Vestal, J. Chem. Phys. 43 (1965) 1356.
[23] M.L. Vestal, J.H. Futrell, J. Chem. Phys. 52 (1970) 978.
[24] S.E. Kupriyanov, A.A. Perov, Sov. Phys.-Tech. Phys. 9 (1965) 1018.
[25] S.E. Kupriyanov, A.A. Perov, Sov. Phys.-Tech. Phys. 8 (1964) 618.
[26] P.G. Fournier, J. Fournier, F. Salama, P.J. Richardson, J.H.D. Eland, J. Chem. Phys. 83 (1985) 241.
[27] J.H.D. Eland, F.S. Wort, R.N. Royds, J. Electron Spectrosc. Relat. Phenom. 41 (1986) 297.
[28] L.J. Frasinski, K. Codling, P.A. Hatherly, Science 246 (1989) 1029.

[29] C. Backx, M.J. Van der Wiel, J. Phys. B 8 (1975) 3020.
[30] K.E. McCulloh, T.E. Sharp, H.M. Rosenstock, J. Chem. Phys. 42 (1965) 3501.
[31] C. Tian, C.R. Vidal, J. Phys. B 31 (1998) 5369.
[32] C. Tian, C.R. Vidal, J. Chem. Phys. 108 (1998) 927.
[33] C. Tian, C.R. Vidal, J. Phys. B 31 (1998) 895.
[34] W.C. Wiley, I.H. Mclaren, Rev. Sci. Instrum. 26 (1955) 1150.
[35] J. Appell, C. Kubach, Chem. Phys. Lett. 11 (1971) 486.
[36] C. Tian, C.R. Vidal, J. Chem. Phys. 109 (1998) 1704.
[37] H.U. Poll, V. Grill, S. Matt, N. Abramzon, K. Becker, P. Scheier, T.D. Märk, Int. J. Mass Spectrom. 177 (1998) 143.
[38] T. Fiegele, C. Mair, P. Scheier, K. Becker, T.D. Märk, Int. J. Mass Spectrom. 207 (2001) 145.
[39] R. Fuchs, R. Taubert, Z. Naturforsch. 19a (1964) 495.
[40] M.R. Bruce, L. Li, C.R. Sporleder, R.A. Bonham, J. Phys. B 27 (1994) 5773.
[41] I. Ben-Itzhak, S.G. Ginther, K.D. Carnes, Phys. Rev. A 47 (1993) 2827.
[42] N. Duric, I. Cadez, M. Kurepa, Int. J. Mass Spectrom. Ion Proc. 108 (1991) R1.
[43] N. Nishimura, H. Tawara, J. Phys. B 27 (1994) 2063.
[44] H.C. Straub, P. Renault, B.G. Lindsay, K.A. Smith, R.F. Stebbings, Phys. Rev. A 52 (1995) 1115.
[45] C. Ma, M.R. Bruce, R.A. Bonham, Phys. Rev. A 44 (1991) 2921.
[46] B. Brehm, J. Grosser, T. Ruscheinski, M. Zimmer, Meas. Sci. Technol. 6 (1995) 953.
[47] H.C. Straub, D. Lin, B.G. Lindsay, K.A. Smith, R.F. Stebbings, J. Chem. Phys. 106 (1997) 4430.
[48] V. Tarnovsky, A. Levin, H. Deutsch, K. Becher, J. Phys. B 29 (1996) 139.
[49] O.J. Orient, S.K. Srivastava, J. Phys. B 20 (1987) 3923.
[50] H. Chatham, D. Hils, R. Robertson, A. Gallagher, J. Chem. Phys. 81 (1984) 1770.
[51] V. Grill, G. Walder, P. Scheier, M. Kurdel, T.D. Märk, Int. J. Mass Spectrom. Ion Proc. 129 (1993) 31.
[52] V. Grill, G. Walder, D. Margreiter, T. Rauth, H.U. Poll, P. Scheier, T.D. Märk, Z. Phys. D 25 (1993) 217.
[53] B.L. Schram, M.J. Van der Wiel, F.J. de Heer, H.R. Moustafa, J. Chem. Phys. 44 (1966) 49.
[54] R. Fuchs, R. Taubert, Z. Naturforsch. 19a (1964) 1181.
[55] L.J. Frasinski, M. Stankiewicz, K.J. Randall, P.A. Hartherly, K. Codling, J. Phys. B 19 (1986) L819.
[56] J.H.D. Eland, Mol. Phys. 61 (1987) 725.
[57] R. Thissen, J. Delwiche, J.M. Robbe, D. Duflot, J.P. Flament, J.H.D. Eland, J. Chem. Phys. 99 (1993) 6590.
[58] M. Lange, O. Pfaff, U. Müller, R. Brenn, Chem. Phys. 230 (1998) 117.
[59] H. Deutsch, K. Becker, S. Matt, T.D. Märk, Int. J. Mass Spectrom. 197 (2000) 37.
[60] D. Margreiter, H. Deutsch, M. Schmidt, T.D. Märk, Int. J. Mass Spectrom. Ion Proc. 100 (1990) 157.
[61] W. Hwang, Y.-K. Kim, M.E. Rudd, J. Chem. Phys. 104 (1996) 2956.
[62] H. Deutsch, K. Becker, R.K. Janev, M. Probst, T.D. Märk, J. Phys. B 33 (2000) L865.
[63] Y.-K. Kim, W. Hwang, N.M. Weinberger, M.A. Ali, M.E. Rudd, J. Chem. Phys. 106 (1997) 1026.
[64] Y.-K. Kim, M.E. Rudd, Comments At. Mol. Phys. 34 (1999) 309.
[65] P.E.M. Siegbahn, Chem. Phys. 66 (1982) 443.
[66] T.A. Field, J.H.D. Eland, Chem. Phys. Lett. 211 (1993) 436.
[67] M.J. Besnard-Ramage, P. Morin, T. Lebrun, I. Nenner, M.J. Hubin-Franskin, J. Delwiche, P. Lablanquie, J.H.D. Eland, Rev. Sci. Instrum. 60 (1989) 2182.
[68] M. Barat, J.C. Brenot, J.A. Fayeton, Y.J. Picard, Rev. Sci. Instrum. 71 (2000) 2050.